Available online at www.sciencedirect.com
SCIENCE DIRECT®
ELSEVIER
International Journal of Mechanical Sciences 46 (2004) 561–583
International Journal of MECHANICAL SCIENCES
www.elsevier.com/locate/ijmecsci

Collapse mechanisms of sandwich beams with composite faces and a foam core, loaded in three-point bending. Part I: analytical models and minimum weight design

Craig A. Steeves, Norman A. Fleck*

Engineering Department, Cambridge University, Trumpington Street, Cambridge CB2 1PZ, UK

Received 26 November 2003; received in revised form 30 April 2004

Abstract

Analytical predictions are made for the three-point bending collapse strength of sandwich beams with composite faces and polymer foam cores. Failure is by the competing modes of face sheet microbuckling, plastic shear of the core, and face sheet indentation beneath the loading rollers. Particular attention is paid to the development of an indentation model for elastic faces and an elastic–plastic core. Failure mechanism maps have been constructed to reveal the operative collapse mode as a function of geometry of sandwich beam, and minimum weight designs have been obtained as a function of an appropriate structural load index. It is shown that the optimal designs for composite–polymer foam sandwich beams are of comparable weight to sandwich beams with metallic faces and a metallic foam core.

Keywords: Sandwich materials; Indentation; Analytical solutions; Optimisation; Beam; Bending; Buckling failure; Composite materials

1. Introduction

Sandwich beams are used increasingly in applications requiring high bending stiffness and strength combined with low weight. The concept of the structural sandwich beam—the separation of stiff faces by a lightweight core—dates back to the 1820s [1], but the systematic use of sandwich beams and sandwich panels as structural elements only gained acceptance in the middle of the 20th century for aircraft structures. Plantema [2], Allen [3], and more recently Zenkert [1] have summarised the literature on sandwich beams, including a systematic design strategy for stiffness and strength. It has

* Corresponding author. Tel.: +44-1223-332-650; fax: +44-1223-332-662.
E-mail address: naf1@eng.cam.ac.uk (N.A. Fleck).

0020-7403/$ - see front matter © 2004 Elsevier Ltd. All rights reserved.
doi:10.1016/j.ijmecsci.2004.04.003

long been recognised that sandwich beams fail by a number of competing mechanisms; Gibson and Ashby [4] generated collapse mechanism maps for beams in bending to show the dependence of failure mode upon the geometry of beam and the relative strength of the faces and core. Although their approach was first demonstrated for aluminium alloy face sheets and polymeric foam cores, it has since been extended to other combinations such as metallic face sheets and metallic foam cores [5–8]. Failure maps for elastic–brittle sandwich beams have been developed by Sutcliffe and co-workers [9] and by Frostig and co-workers [10]. These are based on the higher-order sandwich theory of Frostig [11–13]; this approach, although mathematically sound, has been largely superseded by finite element codes which allow for geometric and material non-linearity. The current study deals with sandwich beams with a non-linear material response of the core and elastic–brittle faces: the sandwich beams comprise a polymeric foam core and glass fibre–epoxy face sheets, loaded in three-point bending. This material combination finds widespread application in boat and ship building.

The scope of the paper is as follows. The existing literature on the stiffness and strength of simply supported sandwich beams is reviewed. Analytical predictions are derived for the three-point bending strength due to core shear, face microbuckling, face wrinkling and indentation. New models of indentation failure are introduced as previous models are shown to be deficient. (Detailed experimental and numerical results in support of the analytical predictions are also presented in a companion paper [14].) The paper concludes with the development of a failure mechanism map with contours of mass and structural load index. Minimum weight designs are determined as a function of an appropriate structural load index, and are compared with the minimum weight design for sandwich beams with solid aluminium alloy face sheets and foamed aluminium alloy cores.

2. Review of the stiffness and strength of sandwich beams in three-point bending

2.1. Stiffness of sandwich beams

Consider a simply supported sandwich beam loaded in three-point bending as sketched in Fig. 1. Let L be the beam length between the supports, b the width of the beam, c the core thickness, and t_f the face thickness. The relevant material properties for the core are the Young's modulus E_c, shear modulus G_c, compressive strength σ_c, and shear strength τ_c; for the face sheets, the pertinent properties are the compressive strength σ_f and Young's modulus E_f. The transverse mid-point deflection is δ due to an applied transverse load P.

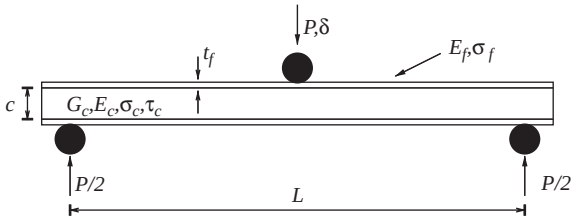

Fig. 1. Geometry of sandwich beam.

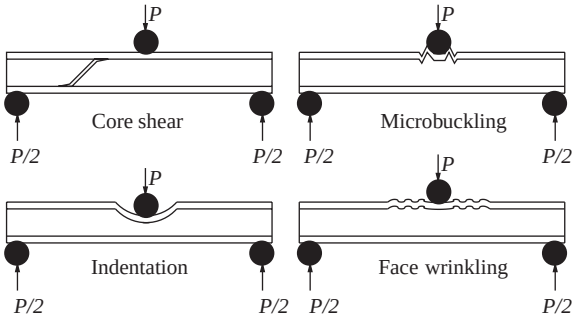

Fig. 2. Competing failure modes of sandwich beams subjected to three-point bending.

Allen [3] gives the total deflection δ at the mid-point of a sandwich beam loaded in three-point bending as the sum of the deflections due to bending of the face sheets and shear of the core:

$$\delta = \frac{PL^3}{48(EI)_{eq}} + \frac{PL}{4(AG)_{eq}}, \tag{1}$$

where $(EI)_{eq}$ is the equivalent flexural rigidity

$$(EI)_{eq} = \frac{E_f b t_f d^2}{2} + \frac{E_f b t_f^3}{6} + \frac{E_c b c^3}{12} \approx \frac{E_f b t_f d^2}{2} \tag{2}$$

and $(AG)_{eq}$ is the equivalent shear rigidity

$$(AG)_{eq} = \frac{bd^2 G_c}{c} \approx bdG_c, \tag{3}$$

in terms of the geometric parameters defined above, and the distance between the centroids of the faces $d = c + t_f$.

2.2. Strength of sandwich beams

Four main modes of collapse have been identified for sandwich beams in three- and four-point bending: face yield, wrinkling of the compressive face sheet, core shear, and indentation beneath the loading rollers, as shown in Fig. 2. These modes of collapse have been confirmed by a number of investigators including Gibson and Ashby [4], Triantafillou and Gibson [15,16], Lingaiah and Suryanarayana [17], Theotokoglou [18], Zenkert [1] and Chen et al. [6]. We review each mode in turn, for the case of a sandwich beam in three-point bending, of geometry sketched in Fig. 1. The strength formulae given below, although approximate, are useful for the construction of collapse mechanism maps and for minimum weight design. For any given sandwich beam under three-point loading, the operative collapse mode is taken to be the weakest mode. For simplicity, interaction between collapse modes is neglected.

2.2.1. Face microbuckling

Microbuckling of composite face sheets occurs when the axial stress within the compressive face sheet attains the face sheet microbuckling strength σ_f. Upon neglecting the contribution of the core

to the overall bending strength, moment equilibrium across the section of the sandwich beam at the location of maximum bending moment implies that the collapse force P is

$$P = \frac{4bdt_f\sigma_f}{L}. \tag{4}$$

It is emphasised that the use of the material parameter σ_f should be treated with caution and used only as a first approximation. It is well known that the fibre microbuckling strength is degraded in the presence of a multi-axial stress state such as that imposed beneath a loading roller (see for example Ref. [19]). Studies by Drapier et al. [20], Wisnom and Atkinson [21], and Fleck and Liu [22] show that the bending strength of composite beams (such as induced by a cylindrical roller) can far exceed the uniaxial compressive strength. Thus, the neglect of face sheet bending beneath the loading roller may be an acceptable assumption. The accuracy of Eq. (4) is explored in the companion paper [14]: experiments support the use of this approximate formula.

2.2.2. Face wrinkling

Face wrinkling is a local elastic instability of the faces involving short wavelength elastic buckling of the upper face sheet, resisted by the underlying elastic core. It may be viewed as the buckling of a beam in axial compression (the face sheet) supported by an elastic foundation (the core).

For sandwich beams with corrugated or honeycomb cores, the core does not constitute a continuous support and the buckling wavelength of the face sheets may scale with the cell size of the core. This phenomenon is known as intercellular buckling, and is considered no further here as it is not relevant to the case of foam-cored sandwich beams.

By treating the core as an elastic half-space, with axial modulus E_c and shear modulus G_c, Hoff and Mautner [23] give a conservative estimate for the face-wrinkling load P as

$$P = \frac{2bt_f d}{L}\sqrt[3]{E_f E_c G_c}. \tag{5}$$

This expression includes a knockdown factor of almost 2 associated with assumed geometrical imperfections of the face sheet [3].

2.2.3. Core shear

In early studies (see Refs. [2,3]) it was assumed that the core collapses at a uniform shear strength τ_c, with negligible additional strength from the face sheets, giving

$$P = 2bd\tau_c. \tag{6}$$

In reality, additional strength is provided by the face sheets. Two limiting cases can be considered: the faces either develop plastic hinges or they continue to bend elastically at collapse of the sandwich beam. For the case of metallic face sheets, plastic hinges have been observed by Chen et al. [6], McCormack et al. [7], and Bart-Smith et al. [24]. To model this case, Ashby et al. [5] have performed an upper bound calculation for rigid, ideally plastic face sheets of yield strength σ_f and a core of shear strength τ_c. The plastic bending strength of the faces elevates the collapse load of the structure by a contribution which scales with the plastic bending moment for the face sheets. Whilst this approach is pertinent to the case of sandwich beams with weak face sheets, it is inappropriate for the case of strong faces—then, plastic shear of the core is accompanied by elastic bending of the face sheets. Chiras et al. [8] have considered this case recently by treating the sandwich beam as

a non-linear Timoshenko beam: for the case of a rigid–ideally plastic core and elastic face sheets, their analysis gives the same yield load as that stated by Eq. (6), with a post-yield hardening response with slope controlled by the bending stiffness of the face sheets. The collapse load in three-point bending, expressed as a function of the mid-point displacement δ is

$$P = 2bd\tau_c + 8E_f b\left(\frac{t_f}{L}\right)^3 \delta. \tag{7}$$

2.2.4. Indentation

In early models of indentation, the face sheets are treated as elastic beams and the core is idealised as an elastic foundation; see, for example, Refs. [11–13,25,26]. However, for most practical sandwich structures, the indentation load is set by plastic yield of the core with the face sheets deforming either elastically or plastically. Triantafillou and Gibson [15,16] assumed that the indentation load is dictated by plastic yield of the core but neglected the contribution to indentation strength from the face sheets. They took the collapse load to equal the uniaxial compressive strength of the core times the loaded area of the core. Whilst this approximation suffices for the case of thin face sheets, it fails for practical sandwich beams: the face sheets provide significant strengthening by a beam-bending action. Limit load expressions for the indentation strength due to the combined plastic collapse of the face sheets and core have been obtained by Ashby et al. [5]. They treat both the face sheets and the core as rigid, ideally plastic solids, with the core undergoing compressive yield, and the face sheets forming plastic hinges. The accuracy of their model was confirmed by a series of experiments and detailed numerical simulations on metallic foam cores and aluminium alloy face sheets; see Refs. [6,7,24].

In the companion paper by Steeves and Fleck [14] it is shown experimentally and by finite element analysis that the indentation load is set by elastic deformation of the faces and compressive yield of the core. This indentation mode has also been observed by Daniel et al. [27]. No theoretical treatment of this collapse mode exists in the literature, to the authors' knowledge; accordingly, a set of indentation models is developed below. The related problem of indentation of an elastic beam upon a plastic foundation has been addressed by Soden [28]. He found that the indentation depth u increases monotonically with indentation load P according to

$$P = \frac{4}{\sqrt{3}}\left(\frac{2}{3}\right)^{1/4} b t_f^{3/4}\sigma_c^{3/4}E_f^{1/4}u^{1/4}. \tag{8}$$

Shuaeib and Soden [29] extended the Soden model to the case of an elastic beam supported by an elastic–ideally plastic core using the analysis of Zingone [30]. The load–displacement response is qualitatively similar but somewhat more compliant than that given by Eq. (8).

The indentation models presented below assume that indentation collapse is a local elastic instability of the compressive face sheet, accompanied by local compressive yielding of the core. Although the overall deformation state within the sandwich beam is much more complex (see Ref. [10] or [31]) than that of the simplified model, the model is expected to be accurate when the peak load is set by a local instability.

The indentation model assumes a transverse instability of the face sheet and not a shear instability. The shear stresses within the core have only a small effect upon the axial force within the face sheet, and are neglected in the analysis. Further, the analysis of Deshpande and Fleck [32] shows that shear straining of the core does not necessarily induce shear stress. They performed triaxial tests

on Divinycell PVC foams and found that compressive yielding is in accordance with a maximum principal stress criterion: a vertex exists along the hydrostatic axis of stress space, and shear straining over a wide range is not sufficient to move the loading point on the yield surface away from this vertex. Thus, the plastically compressed foam core in the indentation zone may provide only normal traction to the face sheet despite the fact that the core is undergoing both deviatoric and hydrostatic straining. The finite element study in the companion paper [14] makes use of the Deshpande–Fleck constitutive model: this constitutive description assumes that PVC foam yields in compression with a vertex along the hydrostatic line. In contrast, previous studies of sandwich beam indentation neglect the presence of the vertex on the yield surface [33].

The analysis given below demonstrates that the presence of large in-plane compressive stresses in the indented face sheet leads to a peak load, as observed experimentally by Daniel et al. [27] and Steeves and Fleck [14]. In version I of the model the core is taken as rigid–ideally plastic, and in version II it is taken as elastic–ideally plastic in order to explore the sensitivity of the indentation response to the elastic compliance of the core, and to justify some of the underlying assumptions of the rigid–ideally plastic core model.

3. Indentation model for elastic face sheets and a rigid–ideally plastic core

Consider the sandwich beam in three-point bending shown in Fig. 1, with elastic faces and a rigid–ideally plastic core of crushing strength σ_c. The transverse load P at mid-span induces a bending moment $M = PL/4$ on the sandwich cross-section at mid-span, and it is assumed that this bending moment is carried by the face sheets. Equilibrium dictates that the upper face sheet is subjected to a compressive axial force $F = M/(c + t_f)$ while the lower face sheet experiences a tensile force of equal magnitude. It is assumed that the foam core compresses beneath the mid-roller in a rigid–ideally plastic manner, so that the transverse line load on the sandwich face from the core is equal to $q = \sigma_c b$, where σ_c is the crushing strength of the core material and b is the width of the beam; see Fig. 3. The length of the indentation zone is 2λ. It is emphasised that the indentation model given here makes no assumption about the variation in normal stress through the thickness c of the core. It simply assumes that the core exerts a normal compressive traction of yield stress magnitude upon the indented portion of the face sheet.

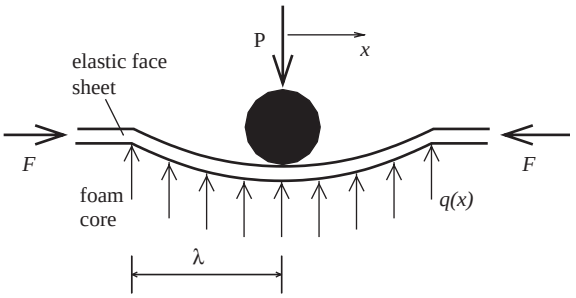

Fig. 3. Indentation zone beneath loading roller.

Consider a typical element of the elastic face sheet subjected to a transverse load per unit length q and to an axial force F; M is the moment on a typical cross-section and V is the shear force. Take x as the distance along the elastic beam and $u(x)$ as the transverse deflection. Then, equilibrium dictates that

$$q = \frac{\mathrm{d}V}{\mathrm{d}x} \tag{9}$$

and

$$F\frac{\mathrm{d}u}{\mathrm{d}x} + V = \frac{\mathrm{d}M}{\mathrm{d}x}. \tag{10}$$

The face sheet bends in accordance with classical beam theory, such that M is related to the curvature, $\mathrm{d}^2u/\mathrm{d}x^2$ by

$$M = -E_f I_f \frac{\mathrm{d}^2u}{\mathrm{d}x^2}, \tag{11}$$

where E_f is the axial modulus of the face sheet and $I_f \equiv bt_f^3/12$ is the second moment of area about its mid-plane.

The governing equation for the beam-column follows from Eqs. (9)–(11) as

$$\frac{\mathrm{d}^4u}{\mathrm{d}x^4} + \frac{F}{E_f I_f}\frac{\mathrm{d}^2u}{\mathrm{d}x^2} = -\frac{q}{E_f I_f}. \tag{12}$$

Note that Eq. (12) does not denote an eigenvalue problem, and admits a solution at all values of F due to the inhomogeneous term on the right-hand side. For the choice $q = \sigma_c b$ the general solution is

$$u = A_1\cos(kx) + A_2\sin(kx) + A_3x + A_4 - \frac{\sigma_c b x^2}{2F}, \tag{13}$$

where A_1, A_2, A_3, and A_4 are constants to be determined and the wave number k is

$$k = \sqrt{\frac{F}{E_f I_f}}. \tag{14}$$

Consider the present problem: the indented face sheet of the sandwich beam is an elastic beam subjected to a uniform line load $q = \sigma_c b$ and to a central transverse load P at the origin $x = 0$, as sketched in Fig. 3. The magnitude of the axial force F follows from moment equilibrium of the sandwich beam in three-point bending:

$$F = \frac{PL}{4d}. \tag{15}$$

We emphasise that the wave number k is dependent upon the in-plane load F and thereby the transverse load P via Eq. (15), and is not to be identified with a foundation modulus. The five unknowns A_1, A_2, A_3, A_4, and λ for the indented face sheet are obtained from the following five boundary conditions:

(i) Symmetry dictates

$$u'(x = 0) = 0. \tag{16}$$

(ii) The shear force on the cross-section of the beam equals $P/2$ at $x = 0$, giving

$$u'''(0) = \frac{P}{2E_f I_f}. \tag{17}$$

(iii) At the end of the indentation zone, the core is rigid, giving

$$u(\lambda) = 0. \tag{18}$$

(iv) The slope at the end of the indented zone vanishes:

$$u'(\lambda) = 0. \tag{19}$$

(v) The moment in the face sheet at the end of the indented zone vanishes since the bending moment is taken to be continuous:

$$u''(\lambda) = 0. \tag{20}$$

(A jump in bending moment at $x = \lambda$ would lead to the unphysical existence of an infinite shear force.) Imposition of boundary conditions (i)–(iii) and (v) leads to the solution

$$A_1 = \frac{2d}{Lk}\left(\frac{1 - \cos\mu - \mu\sin\mu}{\sin\mu - \mu\cos\mu}\right), \tag{21}$$

$$A_2 = -\frac{2d}{Lk}, \tag{22}$$

$$A_3 = \frac{2d}{L}, \tag{23}$$

$$A_4 = \frac{2d}{Lk}\left(\frac{1 - \cos\mu - \mu\sin\mu}{\sin\mu - \mu\cos\mu}\right) + \frac{d\mu^2}{Lk}\left(\frac{1 + \cos\mu}{\sin\mu - \mu\cos\mu}\right), \tag{24}$$

where it is convenient to replace λ by the normalisation $\mu \equiv k\lambda$. The boundary condition (iv), as expressed by Eq. (19), provides an explicit relation between the load P and μ:

$$P = bt_f\left[\frac{4dE_f\sigma_c^2}{3L}\left(\frac{\sin\mu - \mu\cos\mu}{1 - \cos\mu}\right)^2\right]^{1/3}. \tag{25}$$

Similarly, the wavelength $\lambda \equiv \mu/k$ can be expressed in terms of μ by elimination of k through Eqs. (14), (15), and (25) to give

$$\lambda = t_f\mu\left(\frac{dE_f}{6L\sigma_c}\left(\frac{1 - \cos\mu}{\sin\mu - \mu\cos\mu}\right)\right)^{1/3}. \tag{26}$$

The deflection beneath the loading roller $u(0) = A_1 + A_4$ follows from Eqs. (21) and (24) as

$$u(0) = \frac{4d}{Lk}\left(\frac{1 - \cos\mu - \mu\sin\mu}{\sin\mu - \mu\cos\mu}\right) + \frac{d\mu^2}{Lk}\left(\frac{1 + \cos\mu}{\sin\mu - \mu\cos\mu}\right). \tag{27}$$

Thus, the load P, roller displacement $u(0)$ and wavelength λ are each given in terms of the independent parameter μ. Eq. (27) implies that $u(0)$ increases monotonically from zero as μ increases from zero. However, the load P displays a maximum P_{max}, given by

$$P_{max} = bt_f \left(\frac{\pi^2 dE_f \sigma_c^2}{3L} \right)^{1/3}, \tag{28}$$

when μ attains the value π. The corresponding mid-point displacement u_{max} and wavelength λ_{max} are

$$u_{max} = 8t_f \left(\frac{d}{L\pi} \right)^{4/3} \left(\frac{E_f}{3\sigma_c} \right)^{1/3}, \tag{29}$$

and

$$\lambda_{max} = t_f \left(\frac{\pi^2 dE_f}{3L\sigma_c} \right)^{1/3}. \tag{30}$$

A solution exists when $u(0) > u_{max}$, but with a softening response. In subsequent analysis, we make extensive use of the indentation collapse load P_{max} as expressed by Eq. (28).

The assumption that both the slope and the curvature of the face sheet are zero at the position $x = \lambda$ implies that an equilibrating transverse force $V(\lambda)$ is applied to the beam by the foundation at $x = \lambda$. An evaluation of $V(\lambda)$ at the end of the plastic zone gives

$$V(\lambda) = -E_f I_f u'''(\lambda) = -E_f I_f k^3 (A_1 \sin\mu - A_2 \cos\mu), \tag{31}$$

where A_1 and A_2 are given by Eqs. (21) and (22), respectively. The ratio of $V(\lambda)$ to the applied transverse load P is given by

$$\frac{V(\lambda)}{P} = \frac{1}{2} \left(\frac{\mu - \sin\mu}{\sin\mu - \mu\cos\mu} \right) \tag{32}$$

with $V(\lambda)$ acting in the same sense as P. The magnitude $|V(\lambda)/P|$ increases monotonically from zero as μ and $u(0)$ increase from zero; at peak load, μ equals π, and Eq. (32) gives

$$\frac{V(\lambda)}{P} = \frac{1}{2} \left(\frac{\pi - \sin\pi}{\sin\pi - \pi\cos\pi} \right) = \frac{1}{2}. \tag{33}$$

The above analysis can be re-cast in non-dimensional form. Straightforward manipulations reveal that the non-dimensional load $\bar{P}$ and indentation wavelength $\bar{\lambda}$ depend upon the single non-dimensional indentation depth $\bar{u}$ where

$$\bar{P} = \frac{P}{bt_f \sigma_c} \left(\frac{L\sigma_c}{dE_f} \right)^{1/3}, \tag{34}$$

$$\bar{\lambda} = \frac{\lambda}{t_f} \left(\frac{L\sigma_c}{dE_f} \right)^{1/3} \tag{35}$$

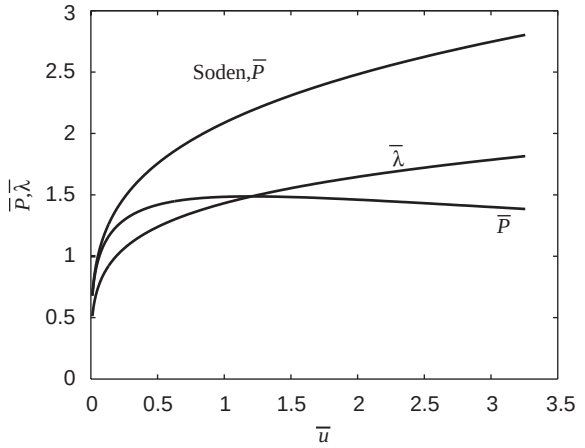

Fig. 4. Indentation response of a sandwich beam with a rigid–ideally plastic core. The curves labelled $\bar{P}$ and $\bar{\lambda}$ refer to the indentation response for a sandwich beam in bending, while the curve labelled 'Soden, $\bar{P}$' refers to a transversely loaded beam on a half-space.

and

$$\bar{u} = \frac{u(0)}{t_f}\left(\frac{L}{d}\right)^{4/3}\left(\frac{\sigma_c}{E_f}\right)^{1/3}. \tag{36}$$

The dependence of $\bar{P}$ and $\bar{\lambda}$ upon $\bar{u}$ is plotted in Fig. 4. The peak load is $\bar{P}_{max} = (\pi^2/3)^{1/3}$, the corresponding wavelength is $\bar{\lambda}_{max} = (\pi^2/3)^{1/3}$, and both are attained at an indentation $\bar{u}_{max} = 8(1/3\pi^4)^{1/3}$. For comparison, $\bar{P}$ is also plotted as a function of $\bar{u}$ for the Soden model; then, the non-dimensional load $\bar{P}$ is an increasing function of $\bar{u}$, given by

$$\bar{P} = \frac{4}{\sqrt{3}}\left(\frac{2}{3}\right)^{1/4}\bar{u}^{\,1/4}. \tag{37}$$

Fig. 5 shows the deflected shape of the compressive face of the sandwich beam under increasing loads, up to the peak value; the axes adopted are $\bar{x} = x\bar{\lambda}/\lambda$ and $\bar{u}_x = u(x)\bar{u}/u(0)$. The rapid increase in beam deflection with increasing load demonstrates the buckling character of the indentation event.

A set of experiments and non-linear finite element simulations support the simple rigid–ideally plastic core indentation model outlined above. In particular, the load versus indentation response and peak load are accurately captured by this analytic approach: see the companion paper by Steeves and Fleck [14].

4. Indentation model for elastic face sheets and an elastic–ideally plastic core

In sandwich beam construction, it is usual for the core to have a much smaller elastic modulus than the face sheets. Consequently, it is anticipated that indentation of the face sheet by the loading roller is accompanied by large elastic strains within the core in addition to the local crush zone immediately below the indenter. In order to assess the significance of elastic compression within the

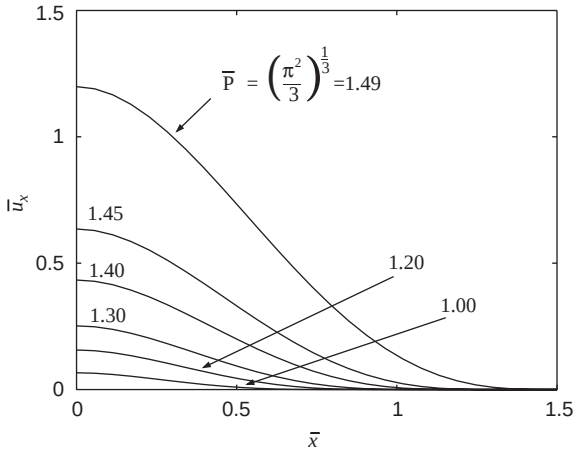

Fig. 5. Deflected shape of the compressive face of a sandwich beam with a rigid–ideally plastic core at selected loads up to the peak value $\bar{P} = 1.49$.

core upon the indentation response, a model is now outlined which treats the core as an elastic–ideally plastic foundation, with an elastic spring stiffness

$$q(x) = su(x), \tag{38}$$

where $q(x)$ is the normal force per unit length exerted by the core on the underside of the face and $u(x)$ is the transverse deflection of the face. It remains to stipulate the magnitude of the foundation stiffness s; here we neglect the variation of normal stress through the thickness of the core and take

$$s \equiv \frac{E_c b}{c}. \tag{39}$$

The core is treated as elastic–ideally plastic with a collapse strength of $q = \sigma_c b$ to be consistent with the rigid–ideally plastic idealisation of Section 3. Thus, the indentation displacement of the core at the onset of core yield is given by

$$u_c = \frac{\sigma_c c}{E_c}. \tag{40}$$

When the load P applied to the sandwich beam in three-point bending is sufficiently small, the indentation response beneath the central loading roller is elastic. The load P versus indentation $u(0)$ response in the elastic regime is calculated by considering the idealised problem of an elastic beam-column for the indented face and an elastic foundation for the core. This problem has been addressed previously by Hetenyi [25] and makes use of the governing equations (9)–(12) with $q = su(x)$. The general solution is

$$u(x) = (B_1 e^{\beta x} + B_2 e^{-\beta x}) \cos(\alpha x) + (B_3 e^{\beta x} + B_4 e^{-\beta x}) \sin(\alpha x), \tag{41}$$

where B_1, B_2, B_3, and B_4 are constants to be determined, and the parameters α and β depend upon the axial load F on the beam-column according to

$$\alpha^2 \equiv \left(\frac{s}{4E_f I_f}\right)^{1/2} + \frac{F}{4E_f I_f} \tag{42}$$

and

$$\beta^2 \equiv \left(\frac{s}{4E_f I_f}\right)^{1/2} - \frac{F}{4E_f I_f}. \tag{43}$$

Recall that F is related to the applied transverse load P via Eq. (15). Imposition of the following boundary conditions:

$$u \to 0 \text{ as } x \to \infty, \tag{44}$$

$$u'(0) = 0 \tag{45}$$

and

$$\int_0^\infty s u(x)\,\mathrm{d}x = \frac{P}{2} \tag{46}$$

provides the solution

$$u(x) = \mathrm{e}^{-\beta x}\left[\frac{P\left(\alpha^2+\beta^2\right)}{4s}\left(\frac{\cos(\alpha x)}{\beta} + \frac{\sin(\alpha x)}{\alpha}\right)\right] \tag{47}$$

with a mid-point displacement

$$u(0) = \frac{P\left(\alpha^2+\beta^2\right)}{4s\beta}. \tag{48}$$

Note that the displacement $u(x)$ is non-linear in load since the parameters α and β depend upon the load P through Eqs. (15), (42), and (43). The indentation compliance at zero load is

$$\left.\frac{\mathrm{d}u(0)}{\mathrm{d}P}\right|_{P=0} = \sqrt{2}\left(\frac{s}{E_f I_f}\right)^{3/4}. \tag{49}$$

Eq. (48) gives the indentation response while the core remains elastic. Yield of the core occurs at $u(0) = u_c = \sigma_c c/E_c$ and the associated yield load P_c is given by the implicit equation

$$P_c = \frac{4\sigma_c b\beta}{\alpha^2+\beta^2}. \tag{50}$$

At loads P above P_c, the core behaves in an elastic–plastic manner, with a central plastic zone at $|x| < \lambda$ and an outer elastic zone over $|x| \geqslant \lambda$. The complete solution is obtained by combining the solution for an elastic beam on a rigid–ideally plastic foundation with the solution for an elastic beam on an elastic foundation. At the elastic–plastic boundary, the deflection of the beam into the foundation $u(\lambda)$ is exactly that needed to produce yield in the core material: $u(\lambda) = \sigma_c c/E_c$.

The governing equations for the beam in the plastic zone $|x| < \lambda$ are given by Eqs. (9)–(12), with the solution

$$u(x) = C_1 \cos(kx) + C_2 \sin(kx) + C_3 x + C_4 - \frac{\sigma_c b x^2}{2F}, \tag{51}$$

in terms of the unknown constants C_1, C_2, C_3, and C_4. Similarly, the governing relations for the elastic region, $|x| \geqslant \lambda$ are given by Eqs. (9)–(12) but with $q = \sigma_c b$ replaced by $q(x) = su(x)$. The solution is

$$\begin{aligned} u(x) = {} & (D_1 e^{\beta(x-\lambda)} + D_2 e^{-\beta(x-\lambda)})\cos(\alpha(x-\lambda)) \\ & + (D_3 e^{\beta(x-\lambda)} + D_4 e^{-\beta(x-\lambda)})\sin(\alpha(x-\lambda)), \end{aligned} \tag{52}$$

where D_1, D_2, D_3, and D_4 are unknown constants and the parameters α and β have been defined in Eqs. (42) and (43). Nine boundary conditions are required to solve for $C_1, C_2, C_3, C_4, D_1, D_2, D_3$, and D_4, and the length of the plastic zone λ. The boundary conditions are

(i) $u \to 0$ as $x \to \infty$, implying that D_1 and D_3 vanish;
(ii) $u = \sigma_c c/E_c$, with continuous $u'(x)$ and $u''(x)$ at the elastic/plastic boundary $x = \lambda$;
(iii) at the origin $x = 0$, $u' = 0$ and $u''' = P/2E_f I_f$;
(iv) overall force equilibrium dictates that

$$\int_0^\infty q(x)\,\mathrm{d}x = \frac{P}{2}. \tag{53}$$

It is again helpful to make the substitution $\mu = k\lambda$ and to solve for $u(x)$ and for the load P in parametric form as functions of the independent variable μ. The solution for the outer elastic zone is

$$D_2 = \frac{\sigma_c c}{E_c} \tag{54}$$

and

$$D_4 = \frac{\alpha^2 + \beta^2}{\alpha}\frac{c}{E_c}\left(\frac{P}{2b} - \sigma_c \lambda\right) - \frac{\sigma_c c \beta}{E_c \alpha}, \tag{55}$$

while the solution for the inner plastic zone is

$$C_1 = \frac{\lambda}{\mu \sin\mu}\left(\frac{\sigma_c c}{E_c}\beta - D_4\alpha - \frac{12\sigma_c\lambda^3}{E_f t_f^3 \mu^2} + \frac{2d}{L}(1-\cos\mu)\right), \tag{56}$$

$$C_2 = -\frac{2d\lambda}{L\mu}, \tag{57}$$

$$C_3 = \frac{2d}{L} \tag{58}$$

and

$$C_4 = \frac{12\sigma_c\lambda^4}{E_f t_f^3 \mu^2} - C_1\cos\mu + \frac{2d\lambda}{L\mu}\sin\mu - \frac{2d\lambda}{L} + \frac{\sigma_c c}{E_c}. \tag{59}$$

Continuity of curvature $u''(x)$ at $x=\lambda$ provides an implicit expression for the plastic zone size λ in terms of μ:

$$\frac{\lambda\tan\mu}{\mu}\left[2D_4\alpha\beta-\frac{\sigma_c c}{E_c}\left(\beta^2-\alpha^2\right)-\frac{2d\mu\sin\mu}{\lambda L}-\frac{12\sigma_c\lambda^2}{E_f t_f^3\mu^2}\right]$$

$$+D_4\alpha-\frac{\sigma_c c}{E_c}\beta+\frac{12\sigma_c\lambda^3}{E_f t_f^3\mu^2}+\frac{2d}{L}(\cos\mu-1)=0, \tag{60}$$

since α and β can each be expressed in terms of μ and λ. The applied transverse load P is given in terms of μ and $\lambda(\mu)$ by making use of Eqs. (14) and (15) and the relation $k=\mu/\lambda$:

$$P=\frac{4dE_f I_f}{L}\left(\frac{\mu}{\lambda}\right)^2. \tag{61}$$

In contrast to the solution for the rigid–ideally plastic core, no explicit algebraic expression can be obtained for the peak load.

Again, it is possible to recast these relations in non-dimensional form. The groups $\bar{P}$, $\bar{u}$, and $\bar{\lambda}$, as defined in Eqs. (34)–(36), are each a function of the non-dimensional independent variable μ, but now an additional independent non-dimensional group is involved:

$$\bar{\Pi}=\frac{\sigma_c}{E_c}\left(\frac{E_c}{E_f}\right)^{1/4}\left(\frac{c}{t_f}\right)^{3/4}\left(\frac{L}{d}\right). \tag{62}$$

The group $\bar{\Pi}$ scales with the yield strain of the core σ_c/E_c, and typical values of $\bar{\Pi}$ range from 0.1 to 1 for composite face sheets and polymeric foam cores. In the limit $\bar{\Pi}\to 0$, the core becomes rigid–ideally plastic and the indentation model given in Section 3 for the rigid–ideally plastic core is recovered. The other limit, $\bar{\Pi}\to\infty$, recovers the Hetenyi elastic core model. The sensitivity to $\bar{\Pi}$ of the collapse response $\bar{P}$ versus $\bar{u}$, and plastic zone size $\bar{\lambda}$ versus $\bar{u}$, is shown in Figs. 6 and 7, respectively. The presence of elastic compliance in the core leads to a small drop in the load carrying capacity of the sandwich beam, and to a decrease in the size $\bar{\lambda}$ of the plastic zone at any given value of $\bar{u}$ relative to the rigid–ideally plastic core.

The effect of the core compliance $\bar{\Pi}$ upon the peak non-dimensional load $\bar{P}_{max}$ is shown in Fig. 8. When $\bar{\Pi}=0$, the rigid–ideally plastic model is recovered, and $\bar{P}_{max}=(\pi^2/3)^{1/3}$. As $\bar{\Pi}$ increases to the value of about 15, $\bar{P}_{max}$ drops to the asymptotic limit given by the Hetenyi model. In the Hetenyi model, yielding of the core is neglected and, as the indentation displacement u increases, the load P asymptotes to the limiting value P_L

$$P_L=\frac{4dbt_f}{L}\left(\frac{E_c E_f t_f}{3c}\right)^{1/2}, \tag{63}$$

which can be re-expressed as

$$\bar{P}_L\bar{\Pi}^{2/3}=\frac{4}{\sqrt{3}}. \tag{64}$$

Typically, for sandwich beams with composite face sheets and polymeric foam cores, $\bar{\Pi}$ lies in the range 0.1–1 and $\bar{P}_{max}$ is adequately approximated by the asymptote $\bar{P}_{max}=(\pi^2/3)^{1/3}$ for the rigid–ideally plastic core. Yielding of the core dominates, and the elastic compliance of the core can be neglected. Within this practical regime of interest, the peak indentation load lies much below the

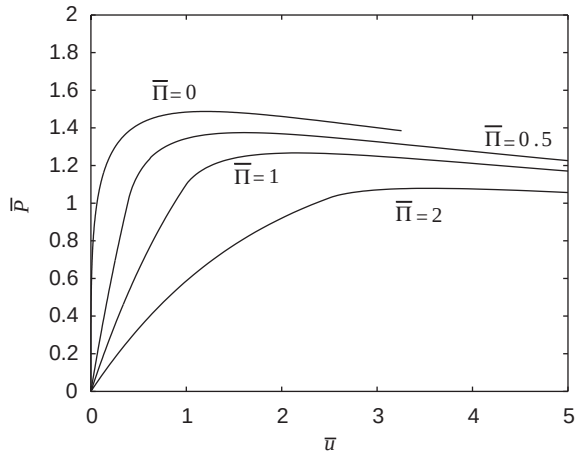

Fig. 6. The effect of core compliance, as parameterised by $\bar{\Pi}$, upon the non-dimensional load versus displacement response for a sandwich beam with an elastic–ideally plastic core; indentation collapse mode.

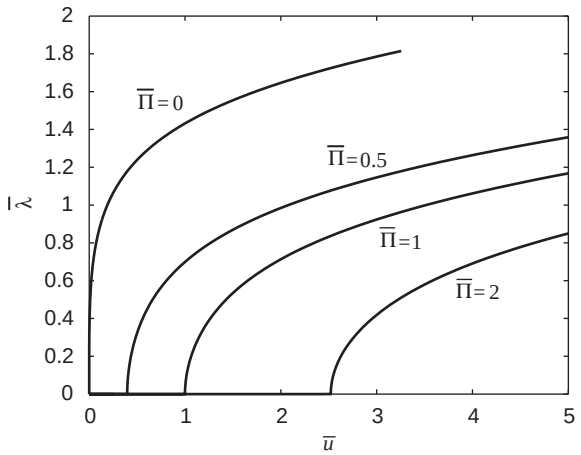

Fig. 7. The effect of core compliance, as parameterised by $\bar{\Pi}$, upon the size of the indentation zone for a sandwich beam with an elastic–ideally plastic core; indentation collapse mode.

Hetenyi result given by Eq. (63) and that of related elastic indentation models, such as Thomsen [26] and Frostig et al. [11].

The effect of core elastic compliance upon the deflected shape of the indented compressive face sheet is shown in Fig. 9, for the choice $\bar{\Pi} = 0.5$. The deflected shape has been plotted using the scaled axes $\bar{u}_x = u(x)\bar{u}/u(0)$ and $\bar{x} = x\bar{\lambda}/\lambda$, for selected values of $\bar{P}$ up to the peak value $\bar{P}_{max} = 1.375$. A comparison of Figs. 9 and 5 shows that the presence of a finite core compliance causes the compressive face to deflect as a damped oscillation in the outer elastic zone. Numerical checks verify that the magnitude of the oscillation is not, in general, sufficient to cause tensile yield of the core within the elastic zone.

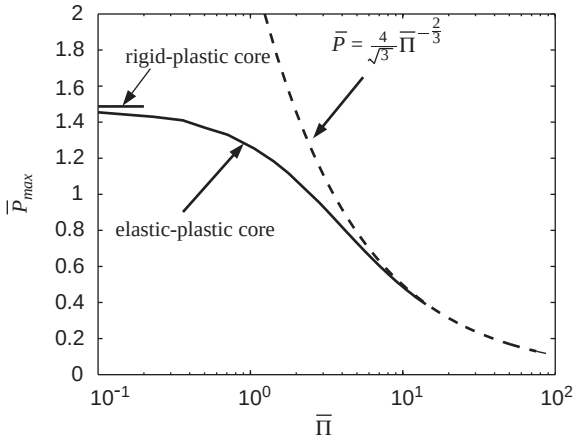

Fig. 8. Dependence of the non-dimensional peak load $\bar{P}_{max}$ upon the compliance $\bar{\Pi}$ for the indentation collapse mode. The dotted line refers to the Hetenyi model.

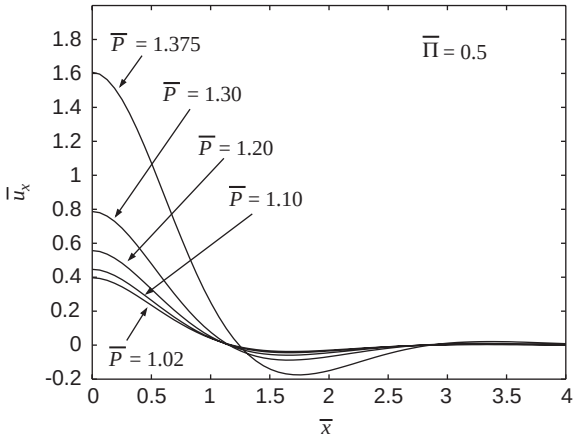

Fig. 9. Deflected shape of the compressive face of a sandwich beam with an elastic–ideally plastic core at selected loads up to the peak load; indentation collapse mode.

Some comment on the assumptions underlying the above indentation models is necessary. It is assumed implicitly that the length of the plastic indentation zone is much smaller than that of the beam. This ensures, first, that the assumption of constant axial force F within the indentation zone is acceptable, and second, that the beam is sufficiently long for localised indentation to occur. For very short beams, failure by overall core crushing is possible, as sketched in Fig. 10. A straightforward estimate of the core-crushing collapse load is

$$P_{cc} = \sigma_c b L. \tag{65}$$

It has also been assumed that the relation between the axial force F and the applied load $P, F = PL/4d$, is specified by the undeformed configuration. In reality, as indentation proceeds, the net

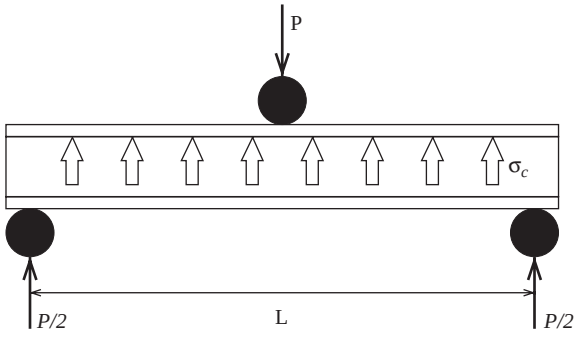

Fig. 10. Core crush of a short sandwich beam.

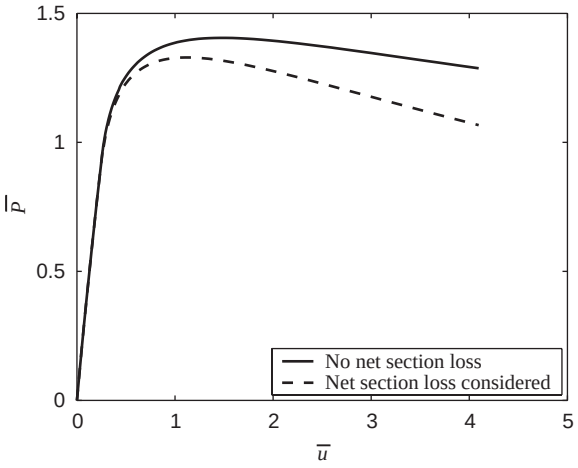

Fig. 11. Effect of net section loss upon the indentation response of a sandwich beam with an elastic–ideally plastic core, $\bar{\Pi} = 0.36$.

section reduces from d to $d-u$; this loss in section progressively magnifies F and thereby destabilises the beam. The significance of this complication is explored in Fig. 11 for the choice $\bar{\Pi} = 0.36$. The calculation involving a progressive loss of section was conducted using an incremental, non-iterative scheme: as μ was incremented, the value of d employed to calculate P and u was taken as $d-u$ where u is the current value. It is found that the loss of section with increasing indentation has only a minor effect upon the collapse response.

5. Minimum weight design and failure mechanism maps

Sandwich beams can be optimised by minimising an objective function such as weight or cost, against a set of constraints such as structural stiffness or strength. Here, we design the geometry of a sandwich beam in three-point bending to achieve minimum mass, against the constraint of

a prescribed structural load index: this is a common optimisation task for sandwich beams. We begin by introducing the structural load index $\widehat{P}$:

$$\widehat{P} = \frac{P}{bL\sigma_f} \tag{66}$$

as an appropriate non-dimensional measure of the sandwich beam strength in three-point bending. The mass M of the sandwich beam is given by

$$M = 2bLt_f\rho_f + bLc\rho_c \tag{67}$$

and is non-dimensionalised to a mass index $\widehat{M}$ where

$$\widehat{M} = \frac{M}{bL^2\rho_f}. \tag{68}$$

It remains to select the geometry of sandwich beam which minimises the mass $\widehat{M}$ for a given structural load index, $\widehat{P}$. The first step is to re-express the collapse load for each competing failure mode in terms of $\widehat{P}$, making use of the following non-dimensional geometrical and material parameters:

$$\bar{t} = t_f/c, \tag{69}$$

$$\bar{c} = c/L, \tag{70}$$

$$\bar{\sigma} = \sigma_c/\sigma_f, \tag{71}$$

$$\bar{\tau} = \tau_c/\sigma_f, \tag{72}$$

$$\bar{E} = E_f/\sigma_f \tag{73}$$

and

$$\bar{\rho} = \rho_c/\rho_f, \tag{74}$$

where ρ_c is the density of the core material and ρ_f is the density of the face material. Then, the load index for face microbuckling follows from Eq. (4) as

$$\widehat{P}_M = 4\bar{t}(\bar{t}+1)\bar{c}^2. \tag{75}$$

In similar fashion, Eq. (6) for core shear and Eq. (28) for indentation failure can be re-expressed as

$$\widehat{P}_{CS} = 2\bar{\tau}(\bar{t}+1)\bar{c} \tag{76}$$

and

$$\widehat{P}_I = \left(\frac{\pi^2\bar{\sigma}^2\bar{E}}{3}\right)^{1/3} \bar{t}(\bar{t}+1)^{1/3}\bar{c}^{4/3}, \tag{77}$$

respectively. Substitution of Eq. (67) into Eq. (68) for the mass index $\widehat{M}$ gives

$$\widehat{M} = (2\bar{t}+\bar{\rho})\bar{c}. \tag{78}$$

In order to deduce the geometrical parameters $\bar{t} = t_f/c$ and $\bar{c} = c/L$ which minimise $\widehat{M}$ for a given $\widehat{P}$ it is helpful to construct a failure mechanism map with axes $\bar{t}$ and $\bar{c}$.

Table 1
Mechanical properties of PVC foams and woven glass–epoxy composite

Material	Compressive strength σ_c (MPa)	Shear strength τ_c (MPa)	Density ρ_c (kg m^{-3})
H30 foam	0.29	0.33	36
H100 foam	1.45	1.60	100
H200 foam	3.85	3.30	200
	Compressive strength σ_f (MPa)	Young's modulus E_f (GPa)	Densityρ_f (kg m^{-3})
GFRP	350	30	1770

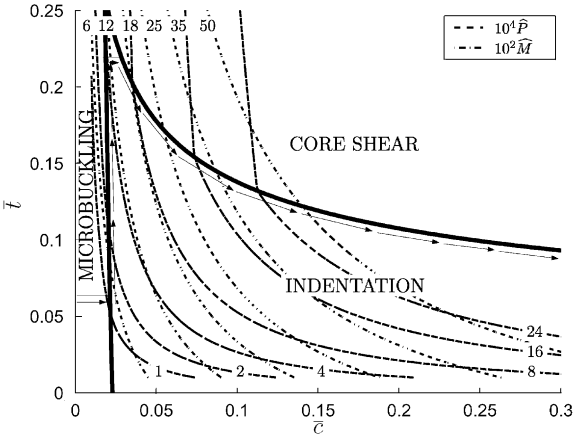

Fig. 12. Failure mechanism map of high-density H200 foam core with contours of mass index $\widehat{M}$ and structural load index $\widehat{P}$, and trajectory of minimum weight design. The solid bold lines denote the boundaries between collapse regimes and the arrows follow the minimum weight trajectory.

This study focusses on sandwich beams with composite faces and polymer foam cores; we therefore take the material properties of three PVC foam cores and a woven glass–epoxy face sheet given in Table 1 as exemplary. (These compositions are addressed experimentally in the companion paper [14].) The failure mechanism maps shown below are unique for each combination of non-dimensional groups $\bar{\sigma}^2\bar{E}$ and $\bar{\tau}$. A typical map is plotted in Fig. 12 for the choice $\bar{\sigma}^2\bar{E} = 0.0104$ and $\bar{\tau} = 0.0094$, which are representative of sandwich beams with glass fibre–epoxy face sheets and the high density Divinycell PVC foam core H200, as detailed in Table 1. Contours of $\widehat{M}$ and $\widehat{P}$ have been added to the collapse mechanism map for $\bar{\rho} = 0.113$. The trajectory of minimum weight design is determined by locating the point $(\bar{c}, \bar{t})$ along each contour of $\widehat{P}$ at which $\widehat{M}$ is a minimum. The minimum weight trajectory is the locus of all such minima. This procedure is straightforward and is performed analytically: algebraic expressions exist for $\widehat{P}(\bar{c}, \bar{t})$ and $\widehat{M}(\bar{c}, \bar{t})$. The details of these calculations are omitted for the sake of brevity. With increasing load index $\widehat{P}$, the trajectory of minimum-weight

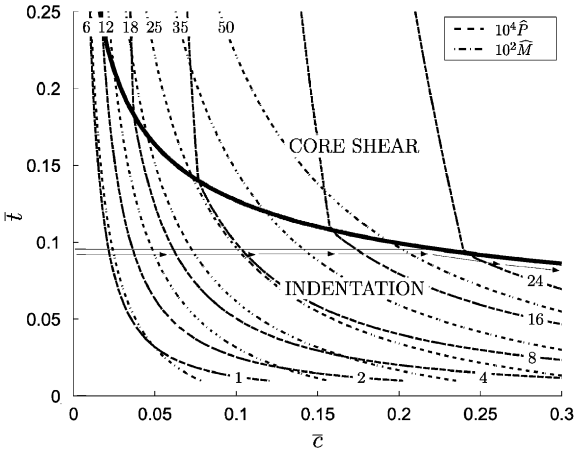

Fig. 13. Failure mechanism map for medium density H100 foam core with contours of mass index $\widehat{M}$ and structural load index $\widehat{P}$. The solid bold line denotes the boundary between the indentation and core shear regimes, and the arrows follow the minimum weight trajectory.

design passes through the microbuckling region, along the boundary between the microbuckling and indentation regimes indicating simultaneous failure by microbuckling and indentation, through the indentation region, and finally along the boundary between the indentation and core shear regimes.

Fig. 13 is a failure mechanism map for a medium density foam core, designated H100 in Table 1, and woven glass–epoxy face sheets, with $\bar{\sigma}^2\bar{E}=0.0015$, $\bar{\tau}=0.0046$, and $\bar{\rho}=0.0565$. A comparison with Fig. 12 reveals that, as the density of the foam core decreases, the microbuckling region disappears and minimum mass designs lie predominantly within the indentation regime. The failure mechanism map for the low density H30 foam core is similar to Fig. 13 for the medium density core, and the minimum weight design trajectory is exclusively within the indentation regime.

The relationship between the minimum mass index $\widehat{M}_{min}$ and the load index $\widehat{P}$ can be stated explicitly for each failure regime. Explicit expressions for the trajectory $(\bar{c},\bar{t})$ as a function of $\widehat{P}$ can also be obtained. In the microbuckling region, we have

$$\widehat{M}_{min}=(\bar{\rho}(2-\bar{\rho})\widehat{P})^{1/2} \tag{79}$$

with the optimal value of $\bar{t}$ given by

$$\bar{t}=\frac{\bar{\rho}}{2(1-\bar{\rho})}. \tag{80}$$

Similarly, within the indentation region, the minimum mass index $\widehat{M}_{min}$ is

$$\widehat{M}_{min}=4\left(\frac{\bar{\rho}(2-\bar{\rho})^3}{9\pi^2\bar{\sigma}^2\bar{E}}\right)^{1/4}\widehat{P}^{3/4} \tag{81}$$

with $\bar{t}$ given by

$$\bar{t}=\frac{3\bar{\rho}}{2\,(1-2\bar{\rho})}. \tag{82}$$

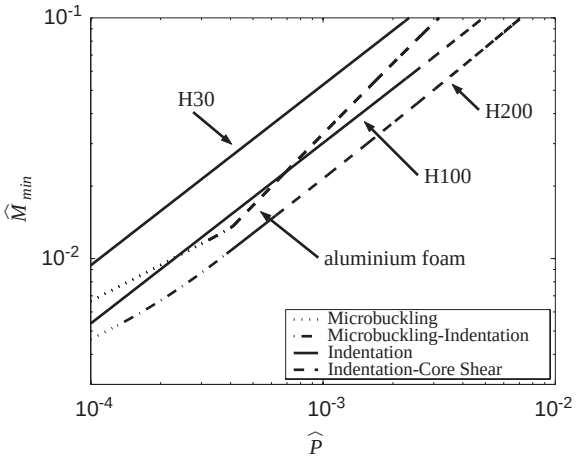

Fig. 14. Dependence of the minimum mass $\widehat{M}_{min}$ upon the structural load index $\widehat{P}$, for composite face sheets and three densities of PVC foam core (H30, H100, and H200), and for an aluminium alloy face sheet and an aluminium alloy foam core. Mass indices for the aluminium sandwich beams are normalised by the density of GFRP.

Along the boundary between the indentation and microbuckling regimes, the minimum mass index $\widehat{M}_{min}$ is stated as

$$\widehat{M}_{min} = \frac{\pi\bar{\rho}\,\bar{\sigma}}{8}\left(\frac{\bar{E}}{3}\right)^{1/2} + \frac{2(2-\bar{\rho})}{\pi\bar{\sigma}}\left(\frac{3}{\bar{E}}\right)^{1/2}\widehat{P}, \tag{83}$$

while along the boundary between the indentation and core shear regimes, $\widehat{M}_{min}$ is

$$\widehat{M}_{min} = \left(\frac{6\bar{\tau}}{\pi^2\bar{\sigma}^2\bar{E}}\right)^{1/3}(2-\bar{\rho})\,\widehat{P}^{2/3} + \frac{\bar{\rho}\widehat{P}}{2\bar{\tau}}. \tag{84}$$

The relationship between $\widehat{M}_{min}$ and $\widehat{P}$ is plotted in Fig. 14 for woven glass–epoxy face sheets and the three densities H30, H100, and H200 of Divinycell PVC foam core, using the properties listed in Table 1. The dependence of the operative failure mode upon $\widehat{P}$ is included in the figure: indentation is the controlling collapse mode for the practical range of values of $\widehat{P}$ for the low foam density, with microbuckling also occurring for the high-density foam. For the practical range of foam densities considered, $\widehat{M}_{min}$ decreases with increasing density of foam core; additional weight reduction may be achieved by the development of higher density foam cores but this is beyond the scope of the present study. It is instructive to compare these minimum weight designs with that obtained previously by Chen et al. [6] for a sandwich beam with an aluminium alloy face sheet and an aluminium alloy foam core ($\bar{\rho}=0.10$, and $\bar{\tau}=\bar{\sigma}=0.0057$). For sandwich beams with ductile faces such as aluminium alloys, the collapse mode of microbuckling is replaced by face yield. The aluminium alloy is assumed to have the same yield strength σ_f as that of the woven composite face sheet. However, aluminium alloys have a density $\rho_{\mathrm{Al}} = 2700\ \mathrm{kg\,m^{-3}}$, which is 50% greater than that of woven composite, $\rho_{comp} = 1770\ \mathrm{kg\,m^{-3}}$. To allow for a fair comparison between the metallic and composite sandwich beams, $\widehat{M}_{min}$ is defined by $\widehat{M}_{min} = M/bL^2\rho_{comp}$ for all sandwich constructions. The minimum weight designs for the aluminium faces and aluminium foam core are included in Fig. 14. It is clear that

the metallic sandwich beam is of similar weight to the composite beam with an H100 PVC foam core; however, the composite beam with an H200 PVC foam core is lighter by a factor of about 2.

6. Concluding remarks

This study has been motivated by a consideration of the collapse strength of sandwich beams with composite face sheets and polymer foam cores; however, the analytical strength formulae developed herein have broader application to the general case of elastic–brittle faces and ductile cores. For example, ceramic faces remain elastic until they crush in axial compression instead of microbuckling, and metallic foam cores collapse plastically.

There are significant differences between the models introduced above and existing models for the indentation strength of sandwich beams. Models which consider an elastic core response, such as the Hetenyi model [25], predict much higher sandwich beam strengths. Alternatively, models which account for core plasticity but do not include axial compression of the face sheet, such as the Soden model [28], also predict higher strengths than the models given here. The indentation models introduced above consider a rigid–ideally plastic core and an elastic–ideally plastic core. The assumption of a rigid–ideally plastic core gives too stiff an initial response but does provide an analytical expression for the peak load in contrast to the model with an elastic–ideally plastic core. It is instructive to construct failure mechanism maps for the competing modes of collapse and to deduce thereby the minimum weight sandwich configuration as a function of structural load index. The comparisons outlined above demonstrate that composite–polymer foam sandwich construction and metallic sandwich construction lead to comparable structural weights for a wide range of loads.

Acknowledgements

The authors are grateful for financial support from the US Office of Naval Research, Contract 0014-91-J-1916.

References

[1] Zenkert D. An introduction to sandwich construction. Sheffield, UK: Engineering Materials Advisory Service; 1995.
[2] Plantema F. Sandwich construction. New York: Wiley; 1996.
[3] Allen H. Analysis and design of structural sandwich panels. Oxford: Pergamon Press; 1969.
[4] Gibson LJ, Ashby MF. Cellular solids. Cambridge: Cambridge University Press; 1988.
[5] Ashby MF, Evans AG, Fleck NA, Gibson LJ, Hutchinson JW, Wadley HNG. Metal foams: a design guide. London: Butterworth, Heinemann; 2000.
[6] Chen C, Harte A-M, Fleck N. The plastic collapse of sandwich beams with a metallic foam core. International Journal of Mechanical Sciences 2001;43(6):1483–506.
[7] McCormack T, Miller R, Kesler O, Gibson L. Failure of sandwich beams with metallic foam cores. International Journal of Solids and Structures 2001;38(28–29):4901–20.
[8] Chiras S, Mumm D, Evans A, Wicks N, Hutchinson J, Dharmasena H, Wadley H, Fichter S. The structural performance of near-optimized truss core panels. International Journal of Solids and Structures 2002;39(15): 4093–115.
[9] Petras A, Sutcliffe M. Failure mode maps in honeycomb sandwich panels. Composite Structures 1999;44(4):237–52.

[10] Shenhar Y, Frostig Y, Altus E. Stresses and failure patterns in the bending of sandwich beams with transversely flexible cores and laminated composite skins. Composite Structures 1996;35(2):143–52.
[11] Frostig Y, Baruch M, Vilnay O, Sheinman I. High-order theory for sandwich-beam behavior with transversely flexible core. Journal of Engineering Mechanics 1992;118(5):1026–43.
[12] Frostig Y, Baruch M. High-order buckling analysis of sandwich beams with transversely flexible core. Journal of Engineering Mechanics 1993;119(3):476–95.
[13] Frostig Y, Baruch M. Localized load effects in high-order bending of sandwich panels with flexible core. Journal of Engineering Mechanics 1996;122(11):1069–76.
[14] Steeves CA, Fleck NA. Collapse mechanisms of sandwich beams with composite faces and a foam core, loaded in three-point bending. Part II: experimental investigation and numerical modelling. International Journal of Mechanical Sciences 2004, in press, doi: 10.1016/j.ijmecsci.2004.04.004.
[15] Triantafillou T, Gibson L. Failure mode maps for foam core sandwich beams. Materials Science and Engineering 1987;95:37–53.
[16] Triantafillou T, Gibson L. Minimum weight design of foam core sandwich panels for a given strength. Materials Science and Engineering 1987;95:55–62.
[17] Lingaiah K, Suryanarayana BG. Strength and stiffness of sandwich beams in bending. Experimental Mechanics 1991;31(1):1–7.
[18] Theotokoglou E. Analytical determination of the ultimate strength of sandwich beams. Applied Composite Materials 1996;3:345–53.
[19] Fleck N. Compressive failure in fiber composites. Advances in Applied Mechanics 1997;33:43–117.
[20] Drapier S, Gardin C, Grandidier J-C, Potier-Ferry M. Structure effect and microbuckling. Composites Science and Technology 1996;56(7):861–7.
[21] Wisnom MR, Atkinson JW. Constrained buckling tests show increasing compressive strain to failure with increasing strain gradient. Composites—Part A: Applied Science and Manufacturing 1997;28(11):959–64.
[22] Fleck N, Liu D. Microbuckle initiation from a patch of large amplitude fibre waviness in a composite under compression and bending. European Journal of Mechanics A/Solids 2001;20:23–37.
[23] Hoff NJ, Mautner SE. Buckling of sandwich type panels. Journal of the Aeronautical Sciences 1945;12(3):285–97.
[24] Bart-Smith H, Hutchinson J, Evans A. Measurement and analysis of the structural performance of cellular metal sandwich construction. International Journal of Mechanical Sciences 2001;43(8):1945–63.
[25] Hetenyi M. Beams on elastic foundation. Ann Arbor: University of Michigan Press; 1946.
[26] Thomsen O. Localised loads. In: Zenkert D, editor. An introduction to sandwich construction. Sheffield, UK: Engineering Materials Advisory Services; 1995 [chapter 12].
[27] Daniel I, Abot J, Wang K-A. Testing and analysis of composite sandwich beams. In: Proceedings of the 12th International Conference on Composite Materials, ICCM; 1999.
[28] Soden P. Indentation of composite sandwich beams. Journal of Strain Analysis 1996;31(5):353–60.
[29] Shuaeib F, Soden P. Indentation failure of composite sandwich beams. Composites Science and Technology 1997;57:1249–59.
[30] Zingone G. Limit analysis of a beam in bending immersed in an elasto-plastic medium. Meccanica 1968;3:48–56.
[31] Thomsen O, Frostig Y. Localized bending effects in sandwich panels: photoelastic investigation versus high-order sandwich theory results. Composite Structures 1997;37(1):97–108.
[32] Deshpande V, Fleck N. Multiaxial yield behaviour in polymer foams. Acta Materialia 2001;49(10):1859–66.
[33] Schwarts-Givli H, Frostig Y. High-order behaviour of sandwich panels with a bilinear transversely flexible core. Composite Structures 2001;53(1):87–106.